ROYAL SOCIETY OF CHEMISTRY

## PAPER

Check for updates

# Analysis of indoor secondary organic aerosol formation near occupants in a classroom using computational fluid dynamics simulations†

Suwhan Yee,[a] Youngbo Won,[a] Bryan Cummings, [b] Michael Waring, [b]
William P. Bahnfleth[a] and Donghyun Rim [*a]

Secondary organic aerosol (SOA) forms indoors when ozone reacts with terpenes, generating a range of low- and semi-volatile compounds, over 50% of which partition into the particle phase. This study investigated the formation of SOA in indoor spaces under heterogeneous thermal conditions resulting from the combined effects of HVAC systems and heat emitted by human occupants. The core of this study involved integrating the volatility basis set (VBS) model with computational fluid dynamics (CFD) simulations. The resulting VBS-CFD framework was used to simulate SOA formation from ozone-terpene reactions, with terpenes originating from human emissions. Model accuracy was assessed using experimental data from previous measurement studies and a material balance model. Results indicate that semi-volatile compound concentrations are substantially higher near occupants compared to ambient levels, while SOA concentrations are lower near humans due to temperature gradients. The study results further revealed notable spatial variability in SOA concentrations under both cooling and heating scenarios, despite maintaining a consistent average indoor temperature. These findings highlight the important role of semi-volatile compounds in influencing particle concentrations near occupants, with over 50% of these compounds potentially contributing to aerosol formation—and thereby increasing human exposure to indoor aerosols.

### Environmental significance

This research examines the formation of secondary organic aerosol (SOA) within indoor environments, employing an integrated methodology that combines volatility basis set (VBS) and computational fluid dynamics (CFD) modeling. Whereas traditional VBS models provide a single, representative concentration value for an entire room, this integrated approach herein uncovers variations in SOA concentrations arising from indoor temperature gradients and airflow dynamics. These findings highlight the necessity for advanced modeling techniques in the effective management of indoor air quality and elucidate the impact of human presence on indoor air pollution. Furthermore, previous models primarily revealed average SOA concentrations under the assumption of well-mixed indoor environments, offering limited insight into spatial variability. By addressing these limitations, the present results demonstrate how the integrated methodology can capture more realistic spatial differences in pollutant concentrations, thereby enhancing air quality control strategies and extending the understanding provided by earlier studies. Notably, the CFD simulations show that, even under a single set-point room temperature, the average SOA concentration can differ depending on the airflow of the space operating under cooling or heating conditions, suggesting the influence of thermal stratification on chemical processes and reinforcing the need for spatially resolved CFD–VBS modelling to guide targeted ventilation interventions.

## 1 Introduction

Indoor air quality is closely linked to human health, as people spend the majority of their time indoors.[1] Numerous studies and reviews have linked indoor air quality to human health outcomes, with hazardous chemicals and airborne particles

*aDepartment of Architectural Engineering, Pennsylvania State University, University Park, PA, USA. E-mail: drim@psu.edu*

*bDepartment of Civil, Architectural and Environmental Engineering, Drexel University, Philadelphia, PA, USA*

† Electronic supplementary information (ESI) available. See DOI: https://doi.org/10.1039/d5em00036j

having notable impacts.[2,3] Fine particles in indoor environments have long been a subject of study due to their association with respiratory and cardiovascular diseases.[4,5] Previous research has focused on primary sources of indoor particles,[6–8] which are typically found in higher concentrations near people, resulting in elevated human exposure to toxins.

Early investigations focused on the mechanics of indoor particles using experimental measurements and comparing them to a standard well-mixed model with physical sources and losses.[9,10] Indoor chemical reactions also form particles, motivating the study of chemical emissions from occupants and human activities associated with secondary organic aerosol (SOA) formation.[11–13] Bekö *et al.*[14] measured occupant emissions

**2538** | *Environ. Sci.: Processes Impacts*, 2025, **27**, 2538–2549

This journal is © The Royal Society of Chemistry 2025

by analyzing specific chemical compositions. Liu et al.[15] investigated the impacts of outdoor particles, ventilation, and human activities on indoor chemical concentrations in a classroom, while Tang et al.[16] analyzed specific compositions of volatile compounds emitted by the human body. Lakey et al.[17] established a model for chemical emissions from human subskin to clothing due to the ozone reaction, validating the model against measured concentration data.

Volatile chemicals emitted from the human body contribute to indoor ozonolysis. Consequently, current research efforts are focused on predicting the extent of SOA formation using chemical models and measuring reactions between ozone and organic materials (OM).[18–29] Kruza et al.[30] developed a chemical model capable of calculating ozone removal and aldehyde production on indoor surfaces. Kroll et al.[31] focused on identifying chemical reactions involved in the formation of organic aerosols. Their research covered a range of reactions, including oxidation initiation, reactions involving peroxy radicals and alkoxy radicals, non-oxidative and oxidative processes in particle-phase reactions, and multiple generations of oxidation.

Donahue et al.[32] introduced the volatility basis set (VBS) model for understanding ambient SOA formation. To permit efficient calculation of gas-particle partitioning behavior, the VBS groups organic compounds into bins based on their volatility. Waring, Cummings, et al.[33–36] developed VBS modeling approaches specifically for indoor applications. A strength of the VBS is its ability to capture temperature effects on species volatility and subsequent aerosol partitioning behavior. However, most indoor studies using the VBS model have considered only well-mixed models. While a well-mixed model can provide valuable insights, spatial discrepancies may arise as rooms become larger with more occupants, include non-isothermal jets from supply air, and develop thermal gradients. To investigate the difference in SOA formation due to a non-isothermal indoor environment, factors that can affect the indoor airflow have been examined in the simulation studies. For instance, Wu et al.[37] demonstrated that a room with floor heating and displacement ventilation contains a vertical temperature distribution. Rim[38] also showed that the temperature gradient between a human body surface and ambient air can influence the indoor environment, resulting in buoyancy-driven flow developed in the vicinity of the body. Furthermore, the indoor temperature distribution can vary depending on cooling, heating, and ventilation conditions.

Although the VBS model is a powerful tool for predicting the SOA formation, it remains unclear how the dispersion of occupancy-driven SOA is affected by indoor conditions and influences the exposure to the occupants. Computational Fluid Dynamics (CFD) simulations have been utilized to understand non-uniform thermal and contaminant distributions under various indoor circumstances.[39] Given this background, the objective of this study is to examine the formation of SOA near human occupants affected by indoor cooling and heating conditions based on combining the VBS model with CFD simulation.

## 2 Methods

### 2.1 Analysis of behavior of organic aerosols (OA)

In order to investigate the spatial distributions of organic particles and gases within a ventilated room, we established the VBS framework into a CFD model. The VBS model was used as a reference to predict the bulk thermodynamic behaviors of organic aerosols (OA). In the VBS model, OM is categorized into discrete volatility bins. Volatility is constrained using the effective saturation concentration ($c^*$, µg m$^{-3}$), and $c^*$ bins are typically separated by factors-of-ten for VBS applications on a logarithmic scale. In this study, the VBS had reference (defined at 298 K) $c^*$ bins ranging from 0.01 to 1000 µg m$^{-3}$.[40]

Reaction yields of OM, comprising both gas and particle phases, are applied to calculate the OM concentration for each volatility bin. These concentrations are then used to determine the equilibrium OA concentrations by solving the system of equations considering aerosol mass fraction outlined below:

$$\xi_i = \left(1 + \frac{c_i^*}{C_{OA}}\right)^{-1} \qquad (1)$$

$$C_{OA} = \sum_i \xi_i C_{OM,i} \qquad (2)$$

where, $\xi_i$ is the aerosol mass fraction, $C_{OA}$ is the total indoor mass concentration of OA, and $C_{OM,i}$ is the mass concentration of organic materials in VBS bin $i$. The effect of temperature on OM volatility is captured efficiently in VBS models by using the Clausius–Clapeyron equation to shift the effective volatility of each bin instead of moving OM between bins:

$$c^* = c_0^* \frac{T}{T_0} e^{\left[\frac{\Delta H}{R}\left(\frac{1}{T_0} - \frac{1}{T}\right)\right]} \qquad (3)$$

where, $T$ is the current temperature, $T_0$ is the reference temperature, $c_0^*$ is the volatility at a reference temperature, $\Delta H$ is the enthalpy of evaporation, and $R$ is the ideal gas constant. Temperature changes affect OA concentrations such that warmer air increases OM volatility, so OA concentrations decrease, and cooler temperatures encourage gas-phase OM to condense into the particle phase.

Organic materials are introduced from air flow inlets and the human body. Organic materials and ozone from outdoors are represented as mole fractions in the inlet air. Monoterpenes are applied to human surfaces and generated at a constant rate. The deposition of OA is modeled on room surfaces (walls, floors, ceilings). The deposition of ozone on the surfaces of the clothed occupants is estimated using the following equations.

$$\frac{dC_i}{dt} = -\beta_i C_i \qquad (4)$$

$$\frac{dC_{ozone}}{dt} = -\beta_{ozone} C_{ozone} \qquad (5)$$

where, $C_i$ is the concentration of OA for bin $i$, $\beta_i$ is the deposition rate of OA for a given bin, $C_{ozone}$ is the concentration of ozone, and $\beta_{ozone}$ is the deposition rate of ozone.

This journal is © The Royal Society of Chemistry 2025

*Environ. Sci.: Processes Impacts*, 2025, **27**, 2538–2549 | **2539**

With these source and deposition terms defined, the CFD model simulates outdoor originating OM, as well as OM produced by chemical reactions. For the integration of these equations to the CFD model, outdoor-originating OM along with OM resulting from chemical reactions are simulated using built-in mass transport models. The VBS framework computed the OA concentration by calculating the aerosol mass fraction for each cell. Temperature may vary from one cell to the next in the CFD simulation, resulting in spatially varying OA partitioning. Consequently, eqn (1)–(3) were iteratively solved in each cell during each iteration of the CFD solution. This approach produced a spatial distribution of condensed-phase OA concentration influenced not only by particle transport phenomenon, but also by thermodynamic effects. The iterative coupling process for calculating the aerosol mass fraction involves updating the organic aerosol concentration $C_{OA}^i$ at each step using the previous AMF and total organic matter concentration, with the updated AMF determined by the partitioning equation (Fig. S1†).

## 2.2 Simulation model and mesh generation

A classroom with dimensions of 10 m × 7 m × 3 m (length, width, height)[41] was simulated using commercial CFD software (STAR-CCM+, version 2302).[42] Fig. 1 shows the arrangement of the occupants and the positions of supply diffuser inlets and return outlets. In the classroom, nine students and one instructor generated a total heat flux of 60 W m$^{-2}$ based on ASHRAE standard 55,[43] in which 40% of the heat was applied to the human surface as convective heat, and 60% was evenly applied to room surfaces as radiative heat.[44]

A polyhedral mesh was employed to create a sufficiently detailed mesh near complex geometry elements like occupants, tables, inlets, and outlets. Two prism layers were utilized on most surfaces, with an additional six layers on occupant surfaces, diffusers, and the outlet to capture intricate airflow around chemical, organic materials, and heat sources and sinks. The first prism layer cell height was set to 1.5 mm, and

the $Y+$ value (dimensionless wall distance, which determines the appropriate size of cells near surfaces) was set to 2, as suggested by Pei et al.[45] Consequently, approximately 220 000 cells were generated for the simulation. A *SST K-ω* turbulence model was incorporated into the simulation to calculate air fluctuation.

To validate the quality of the simulation, the Grid Convergence Index (GCI) was used to evaluate mesh-dependent error. The GCI is a standardized metric that quantifies the error band on the grid convergence of the solution. Three systematically refined grids were generated with characteristic cell sizes of 0.20 m, 0.15 m, and 0.113 m, giving a uniform refinement ratio of $r = 1.33$. The average temperature at the exhaust is used to evaluate and the order of convergence was determined *via* Richardson extrapolation.

$$p = \frac{\ln\left(\frac{T_3 - T_2}{T_2 - T_1}\right)}{\ln r} \qquad (6)$$

where, $p$ is the order of convergence, $T_1$, $T_2$, $T_3$ are the temperatures at the exhaust from each grid, and $r$ is refinement ratio.

The temperature at the exhaust from the simulations for each grid was 25.11 °C, 25.13 °C, and 25.22 °C, respectively. GCI on the fine grids can be calculated using the following equation.

$$\mathrm{GCI}_{fine} = \frac{F_s |e|}{r^p - 1} \qquad (7)$$

where, $F_s$ is the factor of safety (1.25 for three or more grids), $|e|$ is the relative error, $r$ is refinement ratio, and $p$ is the order of convergence.

American Society of Mechanical Engineers (ASME) suggests using GCI less than 5% which can be considered good, and the calculated values for the fine grids in this study were 0.9% and 3.6%, indicating acceptable mesh independence. The position and size of the air supply diffusers were determined to ensure adequate air distribution throughout the room. We simulated two representative indoor ventilation strategies: mixing ventilation and displacement ventilation. Mixing ventilation utilizes
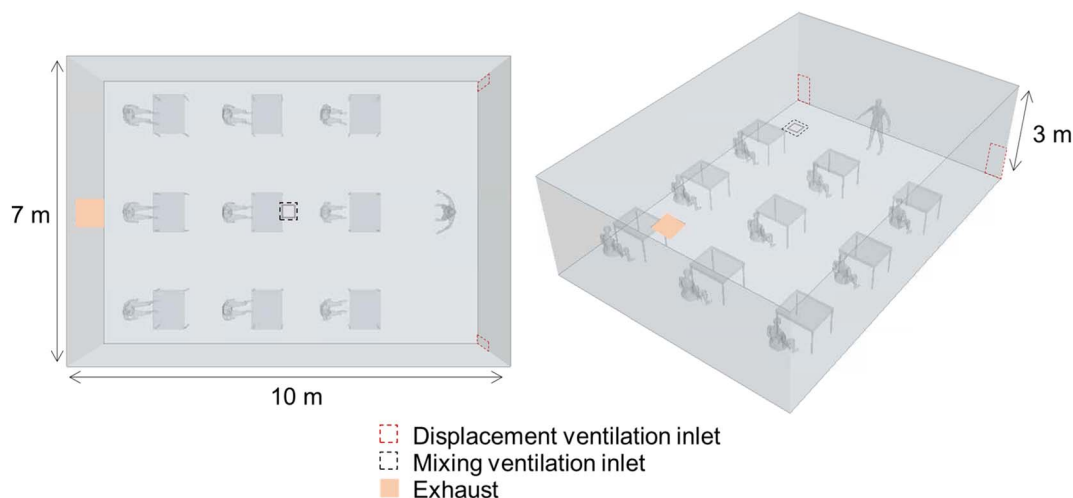


Displacement ventilation inlet
Mixing ventilation inlet
Exhaust

**Fig. 1** A classroom simulation model with ten occupants.

**2540** | *Environ. Sci.: Processes Impacts*, 2025, **27**, 2538–2549

This journal is © The Royal Society of Chemistry 2025

ceiling or wall diffusers to supply air into a space in a way that encourages mixing throughout the room volume. In contrast, displacement ventilation supplies air from the lower portion of the room and discourages mixing and encourages stratification such that air is directed in a uniform direction through and out of the breathing zone. This can be an effective approach for reducing contaminant exposure while efficiently satisfying occupant comfort goals.[46]

In the present study, for mixing ventilation, four-way diffusers with a 30-degree inlet angle were utilized to effectively supply and distribute air. For displacement ventilation, two large diffusers were positioned at the bottom corner of a wall, and the size of the inlets was adjusted to maintain an inlet air speed below 0.5 m s$^{-1}$. For both ventilation strategies, the air exchange rates were established at 1.2 h$^{-1}$ and 0.3 h$^{-1}$ without recirculation. The minimum outdoor air flow rate defined by ASHRAE standard 62.1 (ref. 47) was used to calculate the flow rate that corresponds to 1.2 h$^{-1}$. In this study, 0.3 h$^{-1}$ was also examined to represent a poorly ventilated classroom. To maintain controlled conditions, the average indoor temperature was maintained between 25 and 26 °C.

To incorporate chemical reactions for SOA generation, data on ozone concentration, monoterpenes, and organic aerosol concentrations were integrated into the CFD model. Donahue et al.[32] present atmospheric distributions of organic materials, along with the ratio between gas phase and particle phase. To simulate OM from the outdoors, the OM concentration for the inlet air is determined based on data from each bin, which allows the calculation of OA concentration later in the process. Ozone was introduced from the inlets at a concentration of 30 ppb, according to median outdoor ozone concentration reviewed by Nazaroff et al.[48] Based on previous CFD studies, chemical reactions between ozone and monoterpenes, as well as ozone sinks around the human body, were incorporated into the model.[49–51] The monoterpene emission rate per individual was determined using data from Dornic et al.[52] The monoterpene generation rate was evenly distributed along the occupant body surfaces.

The deposition velocities of particles on the walls and floor were calculated using eqn (8) as per Lai et al.:[53]

$$\beta = \frac{v_d A}{V} \qquad (8)$$

where, $\beta$ is the first order loss rate coefficient, $v_d$ is the deposition velocity, $A$ is the total deposition area, and $V$ is the room volume. For a particle size of 0.1 μm, deposition velocities were 0.0001 cm s$^{-1}$ for the floor and 0.00002 cm s$^{-1}$ for the wall. The choice of particle size of 0.1 μm followed the findings of Huff-Hartz et al.,[54] who reported that nucleated particles generated from the reaction of monoterpenes peak around this size.

### 2.3 Parametric study design

A total of thirty parametric scenarios were designed to explore variations in OM concentration from indoor and outdoor sources and the room's temperature distribution by adjusting the ventilation strategy, air exchange rate, and inlet air

temperature. These simulation cases illustrate how air distribution and occupant activity influence the formation and partitioning of indoor secondary organic aerosols (SOA). The details of these scenarios are summarized in Table 1.

Cases 1–9 represent scenarios without outdoor organic aerosol (OA) contributions, with the total OM concentration in the inlet air set to 0 μg m$^{-3}$. These cases focus on examining SOA formation exclusively from indoor sources. They include simulations under various cooling and heating conditions, featuring different inlet air temperatures and three levels of indoor monoterpene generation. Three inlet air temperatures were applied to establish a temperature gradient across the room. To better isolate and visualize the influence of thermal gradients on indoor airflow behavior, extreme cases with inlet temperatures of 50 °C were included in the analysis. These scenarios were designed to highlight the underlying circulation patterns driven by temperature differences. While such high inlet temperatures are uncommon in real-life indoor environments, they provide valuable insights into the airflow dynamics under intensified heating conditions. However, for all scenarios, the average room temperature was maintained within a range of 25–26 °C by adjusting heat transfer at the room's surfaces, representing heating and cooling scenarios in cold or warm climates. Monoterpene generation by the occupants was configured at three levels: no generation, generation based on the findings of Dornic et al.,[52] and a doubled value compared to the reference.

Cases 10–18 replicate the conditions of cases 1–9, with the exception that the outdoor organic aerosol (OA) concentration is set at 13.5 μg m$^{-3}$. For these cases, the total OM concentration in the inlet air is 30 μg m$^{-3}$, representing 100% of the reference outdoor OA concentration, assuming no filtration of outdoor air. Additionally, cases 19–22 were introduced to evaluate the effects of variability in air exchange rates, while cases 23–26 were designed to compare the differences in secondary organic aerosol (SOA) concentrations between mixing ventilation and displacement ventilation.

### 2.4 Model validation

Two validation procedures were performed with the CFD simulation model after the addition of the VBS model. The first validation model was developed and compared with the chamber test data from other measurement studies to validate the CFD model.[55] Chemical reactions in a 10 m$^3$ test chamber were replicated using the CFD model. The initial α-pinene concentration was set at 13.4 ppb and ozone was injected after the α-pinene concentration had stabilized. The chamber temperature was maintained at 22 °C. The simulation model was pre-run until the indoor airflow and monoterpene concentration had stabilized and then it continued until the chemical reaction between ozone and monoterpenes reached stability. Monoterpenes and ozone reacted and formed 9.6 μg m$^{-3}$ SOA at steady state as a result. The amount of SOA predicted by the CFD simulation was slightly higher than the amount generated from the experiment, which was 6.4 μg m$^{-3}$. However, the two models are in reasonable agreement, with the

This journal is © The Royal Society of Chemistry 2025

*Environ. Sci.: Processes Impacts*, 2025, **27**, 2538–2549 | **2541**

Environmental Science: Processes & Impacts

**Table 1** Simulation cases[a]

| Case | Ventilation strategy | Air exchange rate (h⁻¹) | Inlet air temperature (°C) | Monoterpene generation (µg per m² per day) | Inlet air OM concentration (µg m⁻³) | Heat flux (W m⁻²) |
|---|---|---|---|---|---|---|
| 1 | Mixing | 1.2 | 14 | 0 | 0 | 2.4 |
| 2 | | | 38 | | | −5 |
| 3 | | | 50 | | | −8.3 |
| 4 | | | 14 | 0.73 | | 2.4 |
| 5 | | | 38 | | | −5 |
| 6 | | | 50 | | | −8.3 |
| 7 | | | 14 | 1.43 | | 2.4 |
| 8 | | | 38 | | | −5 |
| 9 | | | 50 | | | −8.3 |
| 10 | | | 14 | 0 | 30 | 2.4 |
| 11 | | | 38 | | | −5 |
| 12 | | | 50 | | | −8.3 |
| 13 | | | 14 | 0.73 | | 2.4 |
| 14 | | | 38 | | | −5 |
| 15 | | | 50 | | | −8.3 |
| 16 | | | 14 | 1.46 | | 2.4 |
| 17 | | | 38 | | | −5 |
| 18 | | | 50 | | | −8.3 |
| 19 | | 0.3 | 14 | 0.73 | 0 | −0.5 |
| 20 | | | 38 | | | −2.46 |
| 21 | | 3 | 14 | | | 8 |
| 22 | | | 38 | | | −11 |
| 23 | Displace-ment | 1.2 | 14 | | | 3.6 |
| 24 | | | 38 | | | −5 |
| 25 | | 0.3 | 14 | | | 0.03 |
| 26 | | | 38 | | | −1.9 |

[a] Heat flux on the surface was calculated to simulate the heat transfer from outside the room. The heat flux is uniformly distributed across the surface. The surface area designated for heat flux measures 224 m².

aerosol mass fraction in the experiment recorded at 0.085, fluctuating within a range of 0.0034 to 0.25 depending on experimental conditions.

Furthermore, the OA concentrations from the CFD simulation were compared with those calculated with the traditional VBS model under a well-mixed condition. The profile of OA mass concentration between the well-mixed VBS model and the proposed CFD approach was not an exact match; however, the OA concentrations were comparable, differing by less than 10%, and the profiles across the volatility bins exhibited notable similarity. Fig. 2 shows the mass concentration of OA due to outdoor OM and SOA formation. The black bars represent the values calculated using the traditional well-mixed VBS approach, while the gray bars show the average concentration from the CFD simulation. Additionally, the error bars indicate the standard deviation of the OA concentration.
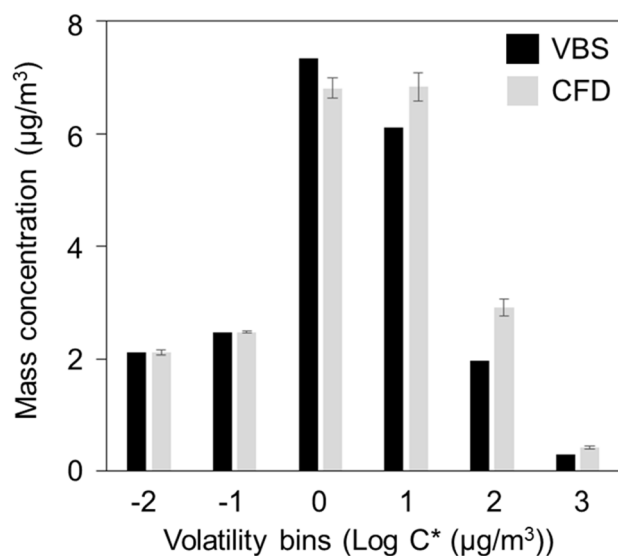
## 3 Results and discussion

### 3.1 Effect of inlet temperature and airflow on spatial distributions of organic aerosols

Fig. 3 illustrates the spatial temperature distributions under mixing ventilation (case 4) and displacement ventilation (case 23). In the case of mixing ventilation, the temperature is relatively uniform throughout the room, with slight variations near the occupants and the inlet, driven by the high-momentum jet of the air supply (see details in Fig. S2†). Conversely, displacement ventilation produces a vertically stratified temperature profile due to the lower velocity and cooler, denser supply air introduced at floor level. This configuration promotes the upward displacement of air, influenced by the inlet air and further enhanced by the thermal plumes generated by the occupants.
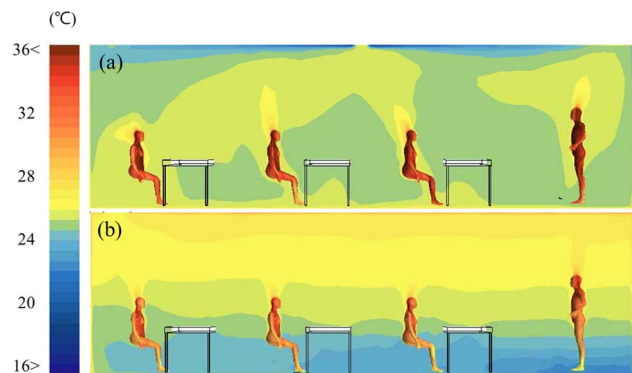


**Fig. 2** Comparison of mass concentration of secondary organic aerosol in six volatility bins between the proposed CFD approach and a traditional well-mixed VBS model.

2542 | *Environ. Sci.: Processes Impacts*, 2025, **27**, 2538–2549

This journal is © The Royal Society of Chemistry 2025

Fig. 3 Temperature distribution under cooling condition with an air exchange rate of 1.2 h$^{-1}$: (a) mixing ventilation (case 4) and (b) displacement ventilation (case 23).

Fig. 4a shows a relatively uniform Secondary Organic Aerosol (SOA) concentration under mixing ventilation compared to the more stratified distribution observed with displacement ventilation in Fig. 4b. However, regardless of the ventilation strategy, SOA concentrations near the occupants are consistently lower than those in the ambient room air. This reduction is primarily attributed to the increased volatility of organic materials at elevated body temperatures and the depletion of ozone in the vicinity of the occupants. Further analysis of SOA volatility reveals that particle-phase SOA concentrations are predominantly concentrated in two volatility bins, specifically where log $c^*$ is 0 and 1, classifying them as semi-volatile organic compounds (see details in Fig. S3†).

The results indicate that the formation of indoor SOA is influenced by the room's temperature gradient and airflow dynamics, with distinct SOA concentration distributions observed near occupants under mixing and displacement ventilation. These variations in OA concentrations under different ventilation strategies are consistent with findings from Pereira et al.[56] Furthermore, the integration of the CFD and VBS models provides a valuable tool for examining indoor conditions, particularly in scenarios involving displacement ventilation and temperature stratification up to 8 °C m$^{-1}$, as observed by Möhlenkamp et al.,[57] or in larger structures with steeper temperature gradients, as described by Gil-Lopez et al.[58] This approach offers a more comprehensive understanding of SOA dynamics in a range of environmental settings.

Fig. 5 illustrates the ratio of SOA concentration and OM concentration for six volatility bins under a cooling condition. The black bars represent the room average concentrations, whereas the gray bars denote the average concentrations at the human boundary layer. The human boundary layer, comprising grid cells adjacent to the occupants (referred to as the prism layer), was selected to represent the average concentrations near individuals. Six layers of grid cells extending up to 6.6 cm from the human surface (0.0735 m$^3$) were utilized to define this layer. The results illustrate the extent of SOA partitioned from OM sources. For both ventilation strategies, the key volatility bins contributing to SOA formation were those where log $c^*$ is 0 and 1. Minimal SOA was produced in bins where log $c^*$ is less than 0, due to the low concentration of OM. Conversely, bins with log $c^*$ greater than 1 contained significant quantities of OM; however, only a small amount of SOA was observed as most of the material remained in the gas phase. Under displacement ventilation, the average room concentration was lower than that observed with mixing ventilation. This difference is mainly due to the lower concentration near the floor resulting from stratification effects caused by stratification effects from the temperature gradient and airflow patterns. Additionally, SOA and OM concentrations near the occupants were even lower than the room average since the seated occupants were closer to the floor, where concentrations are reduced due to stratification. In the scenarios illustrated in Fig. 5, the concentration
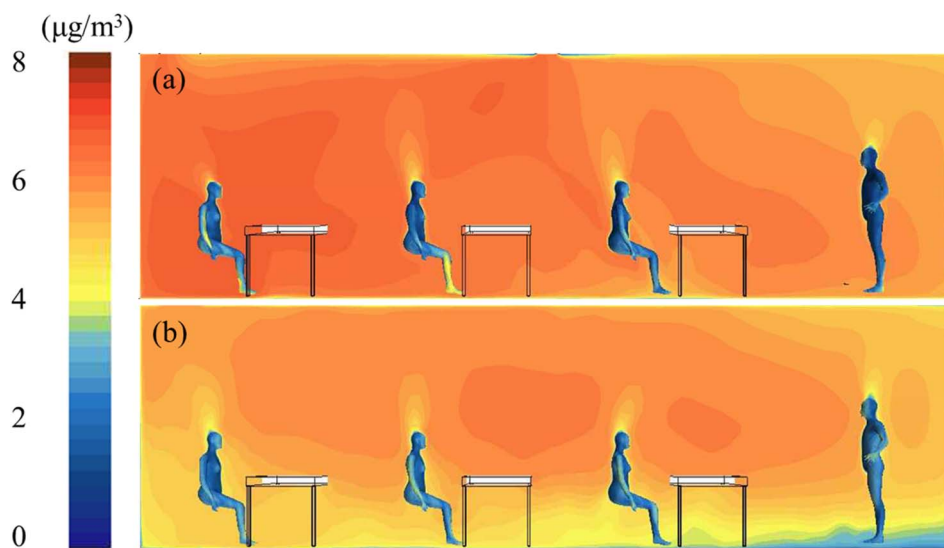


Fig. 4 SOA concentration distribution under cooling condition with an air exchange rate of 1.2 h$^{-1}$: (a) mixing ventilation (case 4) and (b) displacement ventilation (case 23).
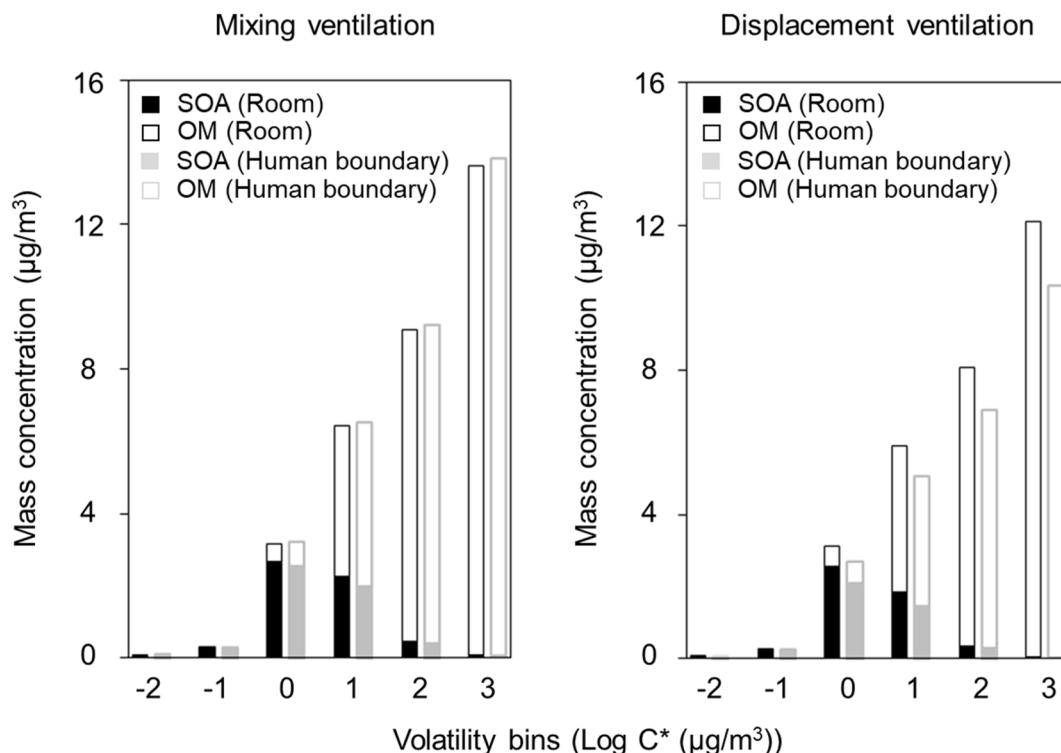
This journal is © The Royal Society of Chemistry 2025

*Environ. Sci.: Processes Impacts*, 2025, **27**, 2538–2549 | **2543**

**Fig. 5** Concentrations of OM and SOA in six volatility bins under cooling conditions with an air exchange rate of 1.2 h$^{-1}$ (cases 4 and 23).

near the occupants was 8.8% lower than the room average under mixing ventilation and 19.3% lower under displacement ventilation. This difference also varied across other cases, depending on the boundary conditions.

The volatility-based analysis reveals how organic materials of different volatilities transition into the particle phase. The concentration of organic materials and organic aerosols across each volatility bin plays a significant role in the disparities observed between different simulation cases. Notably, approximately 75% of the SOA is generated under conditions where $\log c^*$ is 0 and 1, despite only about 30% of the organic materials falling within this range. The SOA concentration was higher in certain spaces in some cases where the airflow is stagnated and the ozonolysis products are accumulated. The results show that OM concentration can vary throughout the room and near occupants, depending on the ventilation strategy and inlet air temperature. These findings suggest that monoterpenes emitted by occupants elevate the concentration of organic compounds in areas where airflow stagnates near the occupants, contributing to higher overall OA concentration within the room. This corroborates that monoterpenes produced by occupants increase the level of semi-volatile organic compounds within the volatility range where the majority of SOA forms, thus raising the OA concentration. Consequently, near the occupants, there was a reduction of up to 24% in OA concentration compared to the average concentration throughout the room.

In addition to the ventilation strategy, supply air temperature can alter indoor airflow patterns and the distribution of indoor SOA concentrations. As the inlet air temperature increases, the buoyancy of the warmer supply air prevents it from reaching the lower sections of the room, as shown in Fig. S5 and S6.† Under cooling conditions, illustrated in Fig. 6a, the room exhibits a relatively uniform SOA concentration. However, under heating conditions, depicted in Fig. 6b and c, the elevated inlet air temperature results in vertical stratification of SOA concentrations. This stratification occurs because
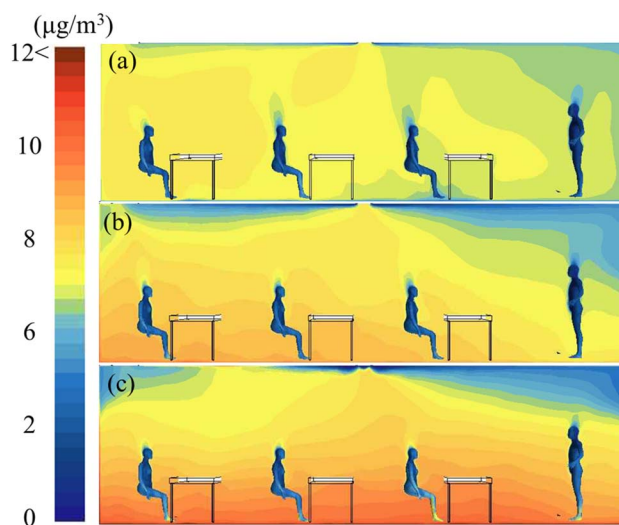


**Fig. 6** Distribution of SOA concentrations under mixing ventilation with an inlet air temperature of (a) 14 °C (case 4, cooling), (b) 38 °C (case 5, heating), (c) 50 °C (case 6, heating).

**2544** | *Environ. Sci.: Processes Impacts*, 2025, **27**, 2538–2549

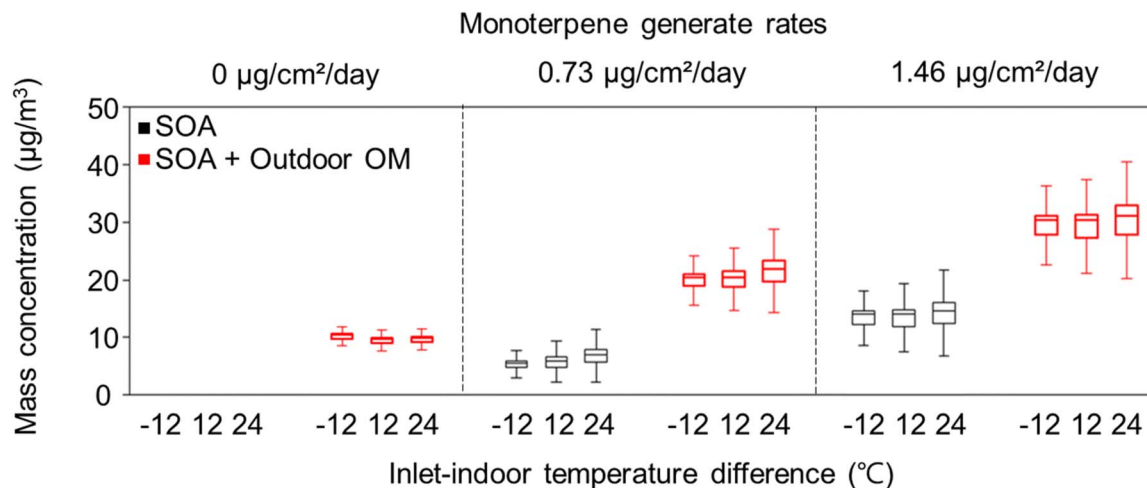This journal is © The Royal Society of Chemistry 2025

**Fig. 7** Organic aerosol (OA) concentrations under different inlet air temperatures and monoterpene generation rates (cases 1–18).

mixing effects are limited to the upper parts of the room, leading to higher SOA concentrations near the floor, where ozonolysis products tend to accumulate.

### 3.2 Effects of indoor and outdoor sources

Indoor organic aerosol (OA) behavior varied under different environmental conditions, including monoterpene generation rates and outdoor organic matter (OM) concentrations. Fig. 7 illustrates the impact of these environmental conditions on OA concentration under mixing ventilation. For a comprehensive comparison, the analysis incorporates both outdoor OM concentration and varying monoterpene generation levels. The black boxplots in Fig. 7 illustrate the spatial range of indoor secondary organic aerosol (SOA) concentrations that are influenced by the ozonolysis of monoterpenes. The box represents the 25th to 75th percentile range, while the error bars indicate the maximum and minimum concentrations, excluding outliers. In the absence of monoterpene generation, indoor SOA concentrations remain at 0 $\mu g\ m^{-3}$. However, when monoterpenes emitted by occupants react with ozone, the average SOA concentration varied with changes in the inlet-indoor temperature differences, ranging from 5.8 $\mu g\ m^{-3}$ to 6.6 $\mu g\ m^{-3}$, with a maximum variation of 13.0%.

When monoterpene generation is doubled to 1.46 $\mu g$ per $m^2$ per day, SOA concentrations increase by 110–150%, fluctuating between 14.1 $\mu g\ m^{-3}$ and 14.5 $\mu g\ m^{-3}$, with a maximum variation of 2.7%. Notably, in scenarios with increased monoterpene production, SOA formation remains unaffected by variations in inlet temperature, unlike the cases with standard monoterpene generation. This occurs because the accumulation of ozonolysis products peaks when ozone is fully depleted. The result suggests that SOA formation becomes independent of indoor cooling and heating conditions when the monoterpene emission rate is elevated, leading to an ozone-limited condition.

The red boxplots in Fig. 7 highlight the total indoor OA concentration, which includes both SOA from the indoor ozonolysis of monoterpenes and outdoor OM concentration (30 $\mu g$

$m^{-3}$). The OA concentration, influenced solely by the outdoor concentration, remains within the range of 9.8 $\mu g\ m^{-3}$ to 10.7 $\mu g\ m^{-3}$, with a maximum variation of about 9.0%. When considering the ozonolysis of monoterpenes from indoors, the OA concentration ranges between 20.8 $\mu g\ m^{-3}$ and 21.7 $\mu g\ m^{-3}$, with a maximum variation of 4.3%. The average increase (10.8 $\mu g\ m^{-3}$) exceeds that observed without outdoor OM concentration (6.1 $\mu g\ m^{-3}$), suggesting that outdoor OM contributes to a higher partitioning of SOA into the particle phase. In the case with a higher monoterpene generation of 1.46 $\mu g$ per $m^2$ per day, the OA concentration ranges between 30.5 $\mu g\ m^{-3}$ and 30.9 $\mu g\ m^{-3}$, with a maximum variation of 1.3%. These findings quantify the influence of both indoor and outdoor aerosol sources on indoor OA concentrations. Furthermore, alterations in indoor OA concentrations were observed in response to varying inlet temperatures, despite a consistent distribution of organic materials across volatility bins, emphasizing the significant impact of indoor heating and cooling conditions on the spatial distribution and thermodynamics of OA.

### 3.3 Effect of ventilation strategy and air exchange rate on OA partitioning

Fig. 8 illustrates the concentrations of OM and their ratios in the particle phase. Under mixing ventilation at a rate of 0.3 $h^{-1}$, the variance in the room-average OM concentration between cooling and heating conditions was approximately 2%. However, when the ventilation rate was increased to 1.2 $h^{-1}$, the difference in the room-average OM concentration between cooling and heating conditions rose to about 10%. In cases with low ventilation, a consistent pattern between heating and cooling conditions was observed, as the long residence time of air allows concentrations to fully equilibrate throughout the space. However, with an increase in the ventilation rate, airflow becomes more prominent due to the influence of inlet air temperature and wall heat transfer, which in turn affects the indoor airflow and transport of organic materials. Under displacement ventilation, the total mass concentrations of
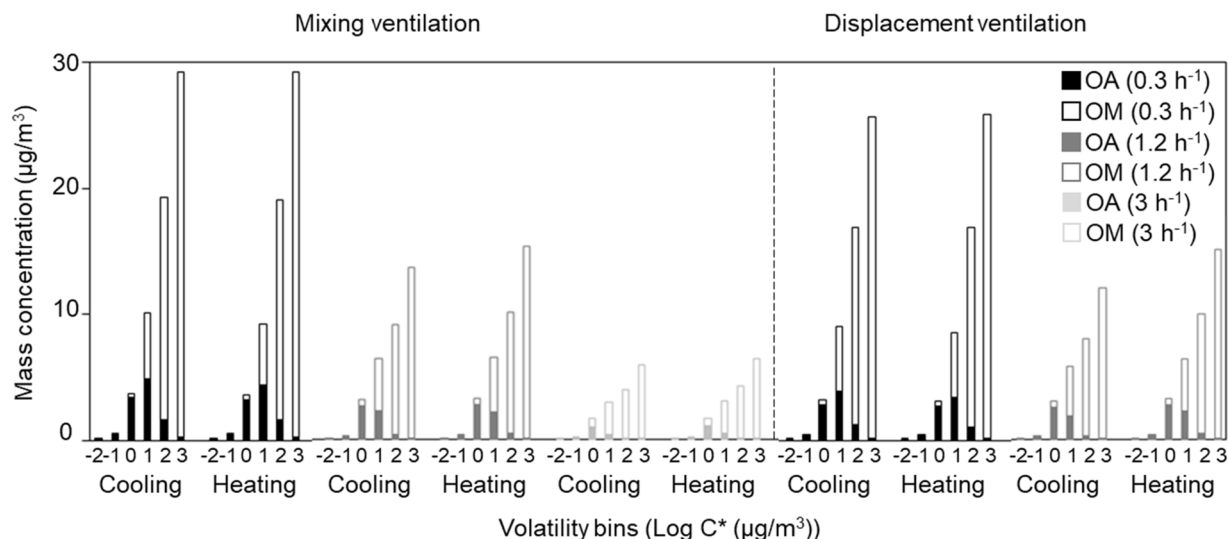
This journal is © The Royal Society of Chemistry 2025

*Environ. Sci.: Processes Impacts*, 2025, **27**, 2538–2549 | **2545**

**Fig. 8** Mass concentrations of organic aerosols (OA) and organic materials (OM) in six volatility bins under different ventilation strategies, inlet air temperature, and air exchange rates (cases 4, 5, and 23–26).

organic materials were up to 14% lower compared to mixing ventilation. Furthermore, the lower concentration of organic materials, combined with a different aerosol mass fraction, led to a reduction in OA concentration by up to 27% (see Fig. S6 for details†).

The differing results between ventilation rates have been observed in previous studies. Sarwar et al.[59] showed that the OA concentration due to SOA formation decreases as the air exchange rate increases, and Coleman et al.[60] revealed that a higher SOA concentration was maintained with the same amount of reactants when the air exchange rate is lowered. Fadeyi et al.[61] compared SOA generation by ozone to show that the generated secondary organic aerosol was diluted by outdoor air under a higher ventilation rate. However, more specific differences can emerge under different simulation conditions. At a ventilation rate of 0.3 h$^{-1}$, mixing ventilation exhibits a wider range of OA concentrations compared to displacement ventilation due to the limited mixing capacity caused by low inlet air speed. In this case, mixing ventilation at a low ventilation rate leaves a larger portion of the indoor space unmixed, increasing the residence time of the room air. In contrast, displacement ventilation transports indoor air with stratification, so a smaller portion of the space has an extended residence time, resulting in a lower average OA concentration due to reduced SOA accumulation.

As the air-exchange rate increases, the differences between ventilation strategies begin to diminish. When the air exchange rate is increased to 1.2 h$^{-1}$, the range of OA concentrations becomes similar for both mixing and displacement ventilation, showing only a minor difference between the two ventilation strategies. At a ventilation rate of 3 h$^{-1}$, mixing ventilation delivers high air exchange that rapidly dilutes both primary OM and newly formed SOA. Furthermore, the high air exchange rate lowered the average aerosol mass fraction from 16.1–17.7% observed at 0.3 and 1.2 h$^{-1}$ to 10.4–11.3%. With an air exchange rate of 1.2 h$^{-1}$, the average OA concentration differs by up to

9.2% between cooling and heating under mixing ventilation, and this discrepancy increases to 19.5% with displacement ventilation. In contrast, at 0.3 h$^{-1}$ the cooling-versus-heating differences drop to only 1.9% for mixing and 0.6% for displacement, while at 3 h$^{-1}$ they remain modest at about 5.4%. These results indicate that unequal mixing has a greater impact near the intermediate air exchange rate of 1.2 h$^{-1}$, suggesting this ventilation level represents a critical regime where thermal stratification formed by different supply air temperatures strongly influences indoor OA distribution.

## 4 Conclusions

A key advancement of this research is the integration of the VBS model with CFD simulations, enabling a more detailed examination of SOA formation across diverse indoor environments. This coupled approach extends beyond the capabilities of traditional models by resolving spatial variability in organic aerosol (OA) concentrations. While the conventional VBS model offers computational efficiency, it lacks the spatial resolution needed to capture localized variations in OA levels. In contrast, the CFD simulations reveal the potential for significant variations in OA levels under different indoor conditions, providing a more comprehensive understanding of SOA dynamics. This integrated approach enables detailed parametric analyses, supporting the investigation of SOA formation and deposition across a range of indoor environments. Specifically, the analysis examines the impacts of ventilation strategies, air exchange rates, indoor chemical sources, and outdoor organic matter (OM) concentrations on indoor SOA formation.

This study demonstrates that when indoor monoterpene emissions are abundant, SOA formation is primarily driven by the concentration of outdoor ozone. In contrast, under low monoterpene emission conditions, indoor factors—such as ventilation strategy, air exchange rate, and supply air temperature—exert a greater influence on SOA levels. Notably, CFD

2546 | Environ. Sci.: Processes Impacts, 2025, **27**, 2538–2549

This journal is © The Royal Society of Chemistry 2025

simulations showed that average SOA concentrations in a room can vary by up to 13%, even when the average room temperature is held constant, depending on whether heating or cooling is applied. Furthermore, the concentration near the occupants was found to be up to 25% lower than the room average depending on the indoor conditions. While the conventional VBS model quickly yields a single result, integrating the VBS model with CFD simulations leverages computational power to uncover distinct SOA formation patterns that are closely linked to airflow dynamics driven by indoor thermal conditions.

While integrating the VBS model into CFD significantly enhances the evaluation of diverse indoor ventilation scenarios, certain limitations remain due to the model's analytical framework. Specifically, the simplification of chemical reactions used in SOA formation calculations prevents the prediction of time-dependent behavior. For instance, Li et al.[62] reported that equilibrium partitioning can take up to 50 minutes under conditions of 298 K and 60% relative humidity, suggesting that SOA partitioning may not respond instantaneously to localized temperature variations captured in the model. In this study, such transient effects are not accounted for, as equilibrium partitioning equations were applied throughout. Also, in scenarios where organic aerosol is highly viscous, elevated near-body temperatures may not lead to evaporation of organic material, and thus, anticipated reductions in exposure may not occur.[63] It also should be noted that particle size distribution was not considered in this study. Particle size was simplified by assuming a single average diameter for all ozonolysis products when estimating the deposition rates. However, particle size distributions resulting from ozone–terpene reactions have been experimentally measured in previous studies.[64] Incorporating aerosol processes such as nucleation and evaporation into CFD simulations may further enhance model fidelity.[65] Future simulations could integrate these experimentally derived size distributions to improve the accuracy and realistic assessments of indoor aerosol behavior.[66] Future research could also explore the complex interactions between human surfaces and their surroundings—including factors such as clothing condition or the material properties of indoor surfaces like flooring and walls—to better understand their role in SOA dynamics and human exposure.

## Data availability

All Raw data for this article are available from the 'ScholarSphere' repository at the PennState.university libraries. **https://scholarsphere.psu.edu/resources/35345235-883c-43d2-a869-ed8d07206c37**.

## Conflicts of interest

There are no conflicts to declare.

## Acknowledgements

## References

1 N. E. Klepeis, W. C. Nelson, W. R. Ott, J. P. Robinson, A. M. Tsang, P. Switzer, J. V. Behar, S. C. Hern and W. H. Engelmann, The National Human Activity Pattern Survey (NHAPS): a resource for assessing exposure to environmental pollutants, *J. Exposure Sci. Environ. Epidemiol.*, 2001, **11**(3), 231–252.

2 J. Sundell, On the history of indoor air quality and health, *Indoor air*, 2004, **14**, 51–58.

3 P. Wolkoff, Indoor air humidity, air quality, and health–An overview, *Int. J. Hyg Environ. Health*, 2018, **221**(3), 376–390.

4 G. Hoek, R. M. Krishnan, R. Beelen, A. Peters, B. Ostro, B. Brunekreef and J. D. Kaufman, Long-term air pollution exposure and cardio-respiratory mortality: a review, *Environ. Health*, 2013, **12**, 1–6.

5 K. L. Jansen, T. V. Larson, J. Q. Koenig, T. F. Mar, C. Fields, J. Stewart and M. Lippmann, Associations between health effects and particulate matter and black carbon in subjects with respiratory disease, *Environ. Health Perspect.*, 2005, **113**(12), 1741–1746.

6 L. Wallace, Indoor particles: a review, *J. Air Waste Manage. Assoc.*, 1996, **46**(2), 98–126.

7 E. Abt, H. H. Suh, G. Allen and P. Koutrakis, Characterization of indoor particle sources: A study conducted in the metropolitan Boston area, *Environ. Health Perspect.*, 2000, **108**(1), 35–44.

8 B. C. Singer, R. Z. Pass, W. W. Delp, D. M. Lorenzetti and R. L. Maddalena, Pollutant concentrations and emission rates from natural gas cooking burners without and with range hood exhaust in nine California homes, *Build. Environ.*, 2017, **122**, 215–229.

9 E. Abt, H. H. Suh, P. Catalano and P. Koutrakis, Relative contribution of outdoor and indoor particle sources to indoor concentrations, *Environ. Sci. Technol.*, 2000, **34**(17), 3579–3587.

10 C. M. Long, H. H. Suh and P. Koutrakis, Characterization of indoor particle sources using continuous mass and size monitors, *J. Air Waste Manage. Assoc.*, 2000, **50**(7), 1236–1250.

11 N. Zannoni, P. S. Lakey, Y. Won, M. Shiraiwa, D. Rim, C. J. Weschler, N. Wang, L. Ernle, M. Li, G. Bekö and P. Wargocki, The human oxidation field, *Science*, 2022, **377**(6610), 1071–1077.

12 J. P. Wong, N. Carslaw, R. Zhao, S. Zhou and J. P. Abbatt, Observations and impacts of bleach washing on indoor chlorine chemistry, *Indoor air*, 2017, **27**(6), 1082–1090.

13 M. S. Waring and J. A. Siegel, Indoor secondary organic aerosol formation initiated from reactions between ozone and surface-sorbed d-limonene, *Environ. Sci. Technol.*, 2013, **47**(12), 6341–6348.

14 G. Bekö, P. Wargocki, N. Wang, M. Li, C. J. Weschler, G. Morrison, S. Langer, L. Ernle, D. Licina, S. Yang and N. Zannoni, The Indoor Chemical Human Emissions and Reactivity (ICHEAR) project: Overview of experimental methodology and preliminary results, *Indoor air*, 2020, **30**(6), 1213–1228.

This journal is © The Royal Society of Chemistry 2025

*Environ. Sci.: Processes Impacts*, 2025, **27**, 2538–2549 | **2547**

15 S. Liu, R. Li, R. J. Wild, C. Warneke, J. A. De Gouw, S. S. Brown, S. L. Miller, J. C. Luongo, J. L. Jimenez and P. J. Ziemann, Contribution of human-related sources to indoor volatile organic compounds in a university classroom, *Indoor air*, 2016, **26**(6), 925–938.

16 X. Tang, P. K. Misztal, W. W. Nazaroff and A. H. Goldstein, Volatile organic compound emissions from humans indoors, *Environ. Sci. Technol.*, 2016, **50**(23), 12686–12694.

17 P. S. Lakey, G. C. Morrison, Y. Won, K. M. Parry, M. von Domaros, D. J. Tobias, D. Rim and M. Shiraiwa, The impact of clothing on ozone and squalene ozonolysis products in indoor environments, *Commun. Chem.*, 2019, **2**(1), 56.

18 C. J. Weschler, Roles of the human occupant in indoor chemistry, *Indoor air*, 2016, **26**(1), 6–24.

19 M. Kruza and N. Carslaw, How do breath and skin emissions impact indoor air chemistry?, *Indoor air*, 2019, **29**(3), 369–379.

20 B. Zhao, S. Wang, N. M. Donahue, W. Chuang, L. Hildebrandt Ruiz, N. L. Ng, Y. Wang and J. Hao, Evaluation of one-dimensional and two-dimensional volatility basis sets in simulating the aging of secondary organic aerosol with smog-chamber experiments, *Environ. Sci. Technol.*, 2015, **49**(4), 2245–2254.

21 B. K. Coleman, H. Destaillats, A. T. Hodgson and W. W. Nazaroff, Ozone consumption and volatile byproduct formation from surface reactions with aircraft cabin materials and clothing fabrics, *Atmos. Environ.*, 2008, **42**(4), 642–654.

22 A. Wisthaler, G. Tamás, D. P. Wyon, P. Strøm-Tejsen, D. Space, J. Beauchamp, A. Hansel, T. D. Märk and C. J. Weschler, Products of ozone-initiated chemistry in a simulated aircraft environment, *Environ. Sci. Technol.*, 2005, **39**(13), 4823–4832.

23 C. M. Salvador, G. Bekö, C. J. Weschler, G. Morrison, M. Le Breton, M. Hallquist, L. Ekberg and S. Langer, Indoor ozone/human chemistry and ventilation strategies, *Indoor air*, 2019, **29**(6), 913–925.

24 C. M. Rosales, J. Jiang, A. Lahib, B. P. Bottorff, E. K. Reidy, V. Kumar, A. Tasoglou, H. Huber, S. Dusanter, A. Tomas and B. E. Boor, Chemistry and human exposure implications of secondary organic aerosol production from indoor terpene ozonolysis, *Sci. Adv.*, 2022, **8**(8), eabj9156.

25 M. O. Fadeyi, C. J. Weschler, K. W. Tham, W. Y. Wu and Z. M. Sultan, Impact of human presence on secondary organic aerosols derived from ozone-initiated chemistry in a simulated office environment, *Environ. Sci. Technol.*, 2013, **47**(8), 3933–3941.

26 T. Joo, J. C. Rivera-Rios, D. Alvarado-Velez, S. Westgate and N. L. Ng, Formation of oxidized gases and secondary organic aerosol from a commercial oxidant-generating electronic air cleaner, *Environ. Sci. Technol. Lett.*, 2021, **8**(8), 691–698.

27 S. Bhangar, J. A. Huffman and W. W. Nazaroff, Size-resolved fluorescent biological aerosol particle concentrations and occupant emissions in a university classroom, *Indoor air*, 2014, **24**(6), 604–617.

28 C. J. Weschler, Chemistry in indoor environments: 20 years of research, *Indoor air*, 2011, **21**(3), 205–218.

29 S. Youssefi and M. S. Waring, Indoor transient SOA formation from ozone+ α-pinene reactions: Impacts of air exchange and initial product concentrations, and comparison to limonene ozonolysis, *Atmos. Environ.*, 2015, **112**, 106–115.

30 M. Kruza, A. C. Lewis, G. C. Morrison and N. Carslaw, Impact of surface ozone interactions on indoor air chemistry: A modeling study, *Indoor air*, 2017, **27**(5), 1001–1011.

31 J. H. Kroll and J. H. Seinfeld, Chemistry of secondary organic aerosol: Formation and evolution of low-volatility organics in the atmosphere, *Atmos. Environ.*, 2008, **42**(16), 3593–3624.

32 N. M. Donahue, A. L. Robinson, C. O. Stanier and S. N. Pandis, Coupled partitioning, dilution, and chemical aging of semivolatile organics, *Environ. Sci. Technol.*, 2006, **40**(8), 2635–2643.

33 B. E. Cummings and M. S. Waring, Predicting the importance of oxidative aging on indoor organic aerosol concentrations using the two-dimensional volatility basis set (2D-VBS), *Indoor air*, 2019, **29**(4), 616–629.

34 M. S. Waring, Secondary organic aerosol in residences: predicting its fraction of fine particle mass and determinants of formation strength, *Indoor Air*, 2014, **24**(4), 376–389.

35 B. E. Cummings, A. M. Avery, P. F. DeCarlo and M. S. Waring, Improving predictions of indoor aerosol concentrations of outdoor origin by considering the phase change of semivolatile material driven by temperature and mass-loading gradients, *Environ. Sci. Technol.*, 2021, **55**(13), 9000–9011.

36 B. E. Cummings, Y. Li, P. F. DeCarlo, M. Shiraiwa and M. S. Waring, Indoor aerosol water content and phase state in US residences: impacts of relative humidity, aerosol mass and composition, and mechanical system operation, *Environ. Sci.: Processes Impacts*, 2020, **22**(10), 2031–2057.

37 X. Wu, B. W. Olesen, L. Fang and J. Zhao, A nodal model to predict vertical temperature distribution in a room with floor heating and displacement ventilation, *Build. Environ.*, 2013, **59**, 626–634.

38 D. Rim, Transient simulation of airflow and pollutant dispersion under mixing flow and buoyancy driven flow regimes in residential buildings, *ASHRAE Trans.*, 2008, **114**, 130.

39 P. V. Nielsen, Fifty years of CFD for room air distribution, *Build. Environ.*, 2015, **91**, 78–90.

40 J. F. Pankow, J. H. Seinfeld, W. E. Asher and G. B. Erdakos, Modeling the formation of secondary organic aerosol. 1. Application of theoretical principles to measurements obtained in the α-pinene/, β-pinene/, sabinene/, Δ3-carene/, and cyclohexene/ozone systems, *Environ. Sci. Technol.*, 2001, **35**(6), 1164–1172.

41 American Society of Heating, Air-Conditioning Engineers, American National Standards Institute, *Thermal Environmental Conditions for Human Occupancy*, American

2548 | *Environ. Sci.: Processes Impacts*, 2025, **27**, 2538–2549

This journal is © The Royal Society of Chemistry 2025

Society of Heating, Refrigerating and Air-Conditioning Engineers, 2004.

42 Siemens Industries Digital Software, *Simcenter STAR-CCM+, version 2302*, Siemens, 2023.

43 Y. Won, P. S. Lakey, G. Morrison, M. Shiraiwa and D. Rim, Spatial distributions of ozonolysis products from human surfaces in ventilated rooms, *Indoor air*, 2020, **30**(6), 1229–1240.

44 G. Pei, M. Taylor and D. Rim, Human exposure to respiratory aerosols in a ventilated room: Effects of ventilation condition, emission mode, and social distancing, *Sustain. Cities Soc.*, 2021, **73**, 103090.

45 G. Pei and D. Rim, Quality control of computational fluid dynamics (CFD) model of ozone reaction with human surface: Effects of mesh size and turbulence model, *Build. Environ.*, 2021, **189**, 107513.

46 G. Cao, H. Awbi, R. Yao, Y. Fan, K. Sirén, R. Kosonen and J. J. Zhang, A review of the performance of different ventilation and airflow distribution systems in buildings, *Build. Environ.*, 2014, **73**, 171–186.

47 American Society of Heating, Refrigerating, Air-Conditioning Engineers, American National Standards Institute, *Ventilation for Acceptable Indoor Air Quality*, American Society of Heating, Refrigerating and Air-Conditioning Engineers, 2001.

48 W. W. Nazaroff and C. J. Weschler, Indoor ozone: Concentrations and influencing factors, *Indoor air*, 2022, **32**(1), e12942.

49 D. Rim, A. Novoselec and G. Morrison, The influence of chemical interactions at the human surface on breathing zone levels of reactants and products, *Indoor Air*, 2009, **19**(4), 324–334.

50 D. Rim, E. T. Gall, S. Ananth and Y. Won, Ozone reaction with human surfaces: Influences of surface reaction probability and indoor air flow condition, *Build. Environ.*, 2018, **130**, 40–48.

51 D. N. Sørensen and C. J. Weschler, Modeling-gas phase reactions in indoor environments using computational fluid dynamics, *Atmos. Environ.*, 2002, **36**(1), 9–18.

52 N. Dornic, A. C. Roudot, A. Batardière, A. S. Nedelec, P. Bourgeois, N. Hornez, F. Le Caer and A. S. Ficheux, Aggregate exposure to common fragrance compounds: Comparison of the contribution of essential oils and cosmetics using probabilistic methods and the example of limonene, *Food Chem. Toxicol.*, 2018, **116**, 77–85.

53 A. C. Lai and W. W. Nazaroff, Modeling indoor particle deposition from turbulent flow onto smooth surfaces, *J. Aerosol Sci.*, 2000, **31**(4), 463–476.

54 K. E. Huff Hartz, T. Rosenørn, S. R. Ferchak, T. M. Raymond, M. Bilde, N. M. Donahue and S. N. Pandis, Cloud condensation nuclei activation of monoterpene and sesquiterpene secondary organic aerosol, *J. Geophys. Res.:Atmos.*, 2005, **110**(D14208).

55 A. A. Presto and N. M. Donahue, Investigation of α-pinene+ ozone secondary organic aerosol formation at low total aerosol mass, *Environ. Sci. Technol.*, 2006, **40**(11), 3536–3543.

56 M. L. Pereira, G. Graudenz, A. Tribess and L. Morawska, Determination of particle concentration in the breathing zone for four different types of office ventilation systems, *Build. Environ.*, 2009, **44**(5), 904–911.

57 M. Möhlenkamp, M. Schmidt, M. Wesseling, A. Wick, I. Gores and D. Müller, Thermal comfort in environments with different vertical air temperature gradients, *Indoor air*, 2019, **29**(1), 101–111.

58 T. Gil-Lopez, M. A. Galvez-Huerta, P. G. O'Donohoe, J. Castejon-Navas and P. M. Dieguez-Elizondo, Analysis of the influence of the return position in the vertical temperature gradient in displacement ventilation systems for large halls, *Energy and buildings*, 2017, **140**, 371–379.

59 G. Sarwar and R. Corsi, The effects of ozone/limonene reactions on indoor secondary organic aerosols, *Atmos. Environ.*, 2007, **41**(5), 959–973.

60 B. K. Coleman, M. M. Lunden, H. Destaillats and W. W. Nazaroff, Secondary organic aerosol from ozone-initiated reactions with terpene-rich household products, *Atmos. Environ.*, 2008, **42**(35), 8234–8245.

61 M. O. Fadeyi, C. J. Weschler and K. W. Tham, The impact of recirculation, ventilation and filters on secondary organic aerosols generated by indoor chemistry, *Atmos. Environ.*, 2009, **43**(22–23), 3538–3547.

62 Y. Li and M. Shiraiwa, Timescales of secondary organic aerosols to reach equilibrium at various temperatures and relative humidities, *Atmos. Chem. Phys.*, 2019, **19**(9), 5959–5971.

63 B. E. Cummings, M. Shiraiwa and M. S. Waring, Phase state of organic aerosols may limit temperature-driven thermodynamic repartitioning following outdoor-to-indoor transport, *Environ. Sci.: Processes Impacts*, 2022, **24**(10), 1678–1696.

64 J. Zhao, J. Ortega, M. Chen, P. H. McMurry and J. N. Smith, Dependence of particle nucleation and growth on high-molecular-weight gas-phase products during ozonolysis of α-pinene, *Atmos. Chem. Phys.*, 2013, **13**(15), 7631–7644.

65 F. Lucci, E. Frederix and A. K. Kuczaj, AeroSolved: Computational fluid dynamics modeling of multispecies aerosol flows with sectional and moment methods, *J. Aerosol Sci.*, 2022, **159**, 105854.

66 Y. Yang and M. S. Waring, Secondary organic aerosol formation initiated by α-terpineol ozonolysis in indoor air, *Indoor Air*, 2016, **26**(6), 939–952.

This journal is © The Royal Society of Chemistry 2025

*Environ. Sci.: Processes Impacts*, 2025, **27**, 2538–2549 | **2549**